Journal of King Saud University – Science 33 (2021) 101339

Contents lists available at ScienceDirect

Journal of King Saud University – Science

journal homepage: www.sciencedirect.com

Modeling cyclic volatile methylsiloxanes removal efficiency from wastewater by ZnO-coated aluminum anode using artificial neural networks

B.S. Reddy [a,1], P.L. Narayana [b,1], A.K. Maurya [b,1], V. Gupta [c], Y.H. Reddy [d], Abdulwahed F. Alrefaei [e], Hussein H. Alkhamis [f], Kwon-Koo Cho [a,*], N.S. Reddy [b,*]

[a] Department of Materials Engineering and Convergence Technology & RIGET, Gyeongsang National University, Jinju, South Korea
[b] School of Materials Science and Engineering, Engineering Research Institute, Gyeongsang National University, Jinju, South Korea
[c] Department of Applied Life Sciences, Gyeongsang National University, Jinju, South Korea
[d] Department of Biomedical Engineering, Amity School of Science and Technology (ASET), Amity University Haryana, 122413, India
[e] Department of Zoology, College of Science, King Saud University, P. O. Box 2455, Riyadh 11451, Saudi Arabia
[f] Department of Botany and Microbiology, College of Science, King Saud University, Riyadh 11451, Saudi Arabia

ARTICLE INFO

Article history:
Received 22 November 2020
Revised 12 December 2020
Accepted 27 December 2020
Available online 7 January 2021

Keywords:
cVMSs removal efficiency
Artificial neural networks
Quantitative
Wastewater
Photo-electrocatalysis

ABSTRACT

Usage of cyclic volatile methyl siloxanes (cVMSs) in the industrial process is unavoidable due to their superior properties; however, it is hazardous to human health. Photocatalytic zinc oxide coated aluminum anode is used to degrade the cVMSs in wastewater. In this work, we investigated the relationship among degradation process parameters such as current density (4–20 mA/cm^2), initial pH (5–9), plate distance (8–24 cm), UV intensity (0–120 W), and reaction time (30–100 min) vis-a-vis cVMSs removal efficiency by using data-driven artificial neural networks(ANN) model. The ANN model was trained using a backpropagation algorithm with the sigmoid activation function between input, hidden, and the output layers. Two hidden layers with eight neurons in each layer presented the minimum average training error (0.24) and higher (0.99) correlation coefficient values (both Pearson's r and Adj. R^2) as compared with the conventional regression model. The effect and relationship between the parameters and cVMSs removal efficiency were analyzed by single, two variable sensitivity analysis, qualitative and quantitative estimation.

1. Introduction

In industrial applications, siloxanes are widely used due to their high compressibility, thermal stability, low flammability, low surface tension, water-repelling properties, and the limited effect of useful temperature properties (Bletsou et al., 2013; Durán et al., 2020). Cyclic volatile methyl siloxanes (cVMSs) such as dodecamethylcyclohexasiloxane, octamethylcyclotetrasiloxane, decamethylcyclopentasiloxane, and chemicals containing Si-O bonds with organic radicals bound to Si including methyl, ethyl groups are widely used in personal care products, pharmaceuticals, and silicone polymer production (Shukla et al., 2011). However, the cVMSs may hazardous to humans and the environment as they reach waterways due to their low degradation rate and bioaccumulation. The wastewater plants (WWTPs) have been verified as a pivotal channel for the cVMSs entry into the environment. The non-volatile silicone fluids are used in polishes, wax, textile applications, cosmetics, and cleaning products end up in wastewater to a large extent. Nearly 200–700 ton/year cVMSs are directly released into the wastewater (Alsamhary, 2020). After the treatment process, approximately 90% of ethyl siloxanes spread on agricultural lands and flow through the sludge, disposed of or incinerated for landfills. In contrast, the remaining 10% still sustain in the waste and pour into the environment. There are many reports on the fate and distribution of the siloxanes in the environment (Bletsou et al., 2013; Guo et al., 2019). Previous stud-

* Corresponding authors.
E-mail addresses: kkcho66@gnu.ac.kr (K.-K. Cho), nsreddy@gnu.ac.kr (N.S. Reddy).
[1] Equally Contributed

Peer review under responsibility of King Saud University.

Production and hosting by Elsevier

https://doi.org/10.1016/j.jksus.2020.101339
1018-3647/

ies on the decomposition and mineralization process of siloxanes mainly focused on clarifying the environment's degradation mechanism or biogas treatment plants (Hori et al., 2019). The methods like electrochemical oxidation, photocatalytic oxidation, ozonation, adsorption, and subcritical water oxidation to remove cVMSs from wastewater.

Understanding the relationship among the degradation process parameters (current density (mA/cm^2), initial pH, UV intensity (W), and reaction time (min)) with cVMSs removal efficiency (%) is essential for efficient processing. To correlate the relationship between these parameters is very challenging and creating a predictive model is crucial. Recently, machine learning (ML) techniques such as ANN are more applicable due to their easy use for prediction. However, the ANN technique is most useful among ML techniques to correlate the relationship between the process variables on the removal efficiency of cVMSs from the wastewater. ML methods were used for continuous activated sludge treatment (Newhart et al., 2020), wastewater treatment plant (Hernández-del-Olmo et al., 2019) and large-scale spatiotemporal characteristics and influence of Yangtze river basin wastewater (Di et al., 2019). Gadekar and Ahammed (2019) used the ANN model for dye removal by adsorption onto water treatment residuals.

Our study was an attempt to develop a systematic ANN framework to determine the relationship among photo-electrocatalysis process parameters on the removal efficiency of cVMSs. The considered process parameters are reaction time, UV intensity, plate distance, initial pH, and current density. The specific objectives of the present work are

- To predict the cVMSs removal efficiency at new unseen experimental conditions.
- To study the influence of individual and the combined effect of process variables on the removal efficiency of cVMSs.
- To develop a user-friendly ANN software for cVMSs removal efficiency for easy use.

2. Materials and methods

2.1. Data collection and ANN model procedure

In the present study, the experimental data for ZnO-coated aluminum anode contains current density, initial pH, plate distance, UV intensity, and reaction time concerning cVMSs removal efficiency (%) collected from previously published literature (Tang et al., 2020). The schematic representation of the present work was shown in Fig. 1. The statistics and the entire database used for the modeling were presented in Table 1 and Table S1, respectively. From the total 50 experimental databases, 80% of datasets were used for model development, and 20% were used to test the model's performance. All the inputs and output variables were normalized between 0.1 and 0.9. The normalization equations and explanations have been mentioned in our earlier reports (Li et al., 2019; Maurya et al., 2020).

The present ANN model and graphical user interface were written in C language and JAVA program (Reddy et al., 2015). The model was trained with the backpropagation algorithm with a sigmoid activation function (LeCun et al., 2015; Lippmann, 1987). This model contains the five neurons in the input layer (current density, plate distance, Initial pH, UV intensity, and reaction time) and one output layer (cVMSs removal efficiency).

2.2. Developing the ANN model

The ANN is typically organized in layers (inputs, hidden, and output layers) and works based on the human brain's operative (Bramer, 2020; Sadan et al., 2016). ANN model was developed

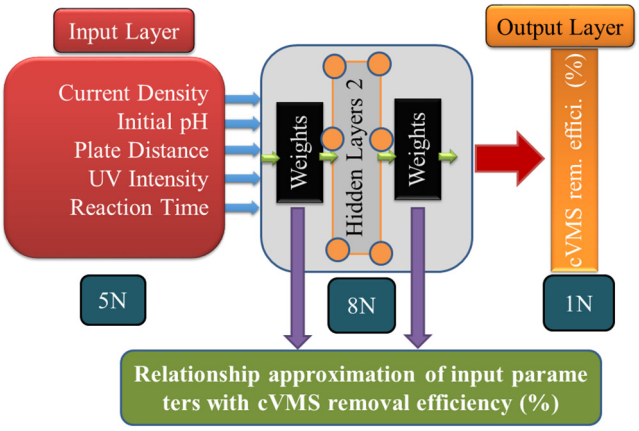

Fig. 1. Schematic representation of the proposed ANN model (5-8-8-1 Architecture).

Table 1
Statistics of the process parameters used in the present study.

Variable	Minimum	Maximum	Mean	Std. dev
Current Density (mA/cm^2)	4	20	12	3.19
Initial pH	5	9	7	0.76
Plate Distance (mm)	8	24	16	3.19
UV Intensity (W)	0	120	60	23.56
Reaction Time (min)	30	100	65	14.03
cVMSs removal efficiency (%)	15.2	64	49.45	10.81

based on three types of exclusive layers; (1) input layer, (2) desired output layer, and (3) hidden layer(s) entirely associated with the neurons. The estimated results are showed the effect and relationship between the input variables and functionalized the results from the unseen database. Within, the experimental data are adjusted by the training and testing. The training database was used for developing the ANN model. To obtain the best structure of the model, we varied the hyperparameters (learning rate, hidden layers, neurons, momentum term, and the number of iterations) and calculated the mean square error (MSE) along with the average error in output predictions (E_{tr}).

In the first, the model was trained with hidden layers (one, two, and three) with a momentum term 0.45, the learning rate 0.6, and 8500 iterations by varying the hidden neurons from 2 to 10. The two hidden layers, with eight neurons, achieved a minimum E_{tr} of 0.475 and RMSE of 0.00002, as shown in Fig. 2(a&b). We selected the two hidden layers with eight hidden neurons in each layer to optimize the other parameters. The momentum term and learning rate was varied from 0.1 to 0.9. We achieved an average error of 0.35 and RMSE of 0.00001 at 0.9 momentum term and 0.5 learning rate, as shown in Fig. 2(c,d,e, and f). Finally, we varied iterations from 0 to 8500 iterations. We achieved the average error, testing, training errors, and RMSE is 0.247, 0.198, 0.44, and 0.00001, respectively, at 8000 iterations, as shown in Fig. 2(g&h). Based on the testing and training errors, we choose the 8000 iterations as an optimum iteration. The 5–8-8–1 ANN architecture with a momentum term of 0.9, the learning rate of 0.5, and 8000 iterations were used for further analysis.

3. Results and discussion

3.1. Distribution of the weights in the ANN model

The established ANN model has 50 datasets; these datasets are associated with some ANN weights and hold some evidence about the connection between process variables and cVMSs removal efficiency. The ANN model's prediction efficiency depends upon the

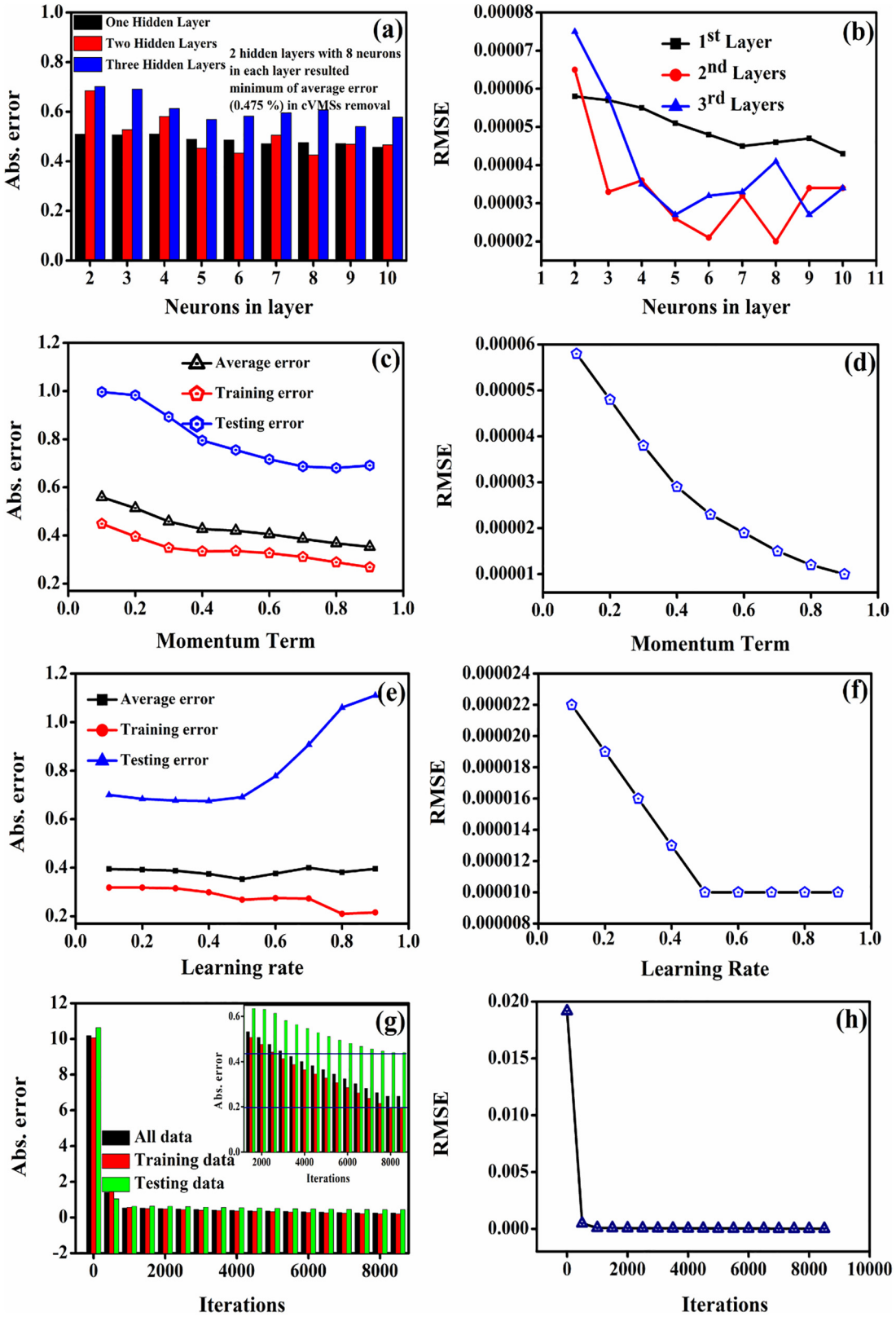

Fig. 2. Average absolute error in prediction (E_{tr}) and RMSE of cVMSs removal efficiency as a function of (a and b) neurons in layers, (c and d) momentum term, (e and f) learning rate, and (g and h) iterations.

magnitude and nature of the distribution of weights (Reddy et al., 2020). Fig. 3(a) shows the initial and best model weights at 8000 iterations. The architecture, 5–8-8–1 yields, a total of 129 weights ((5 + 1) × 8)+((8 + 1) × 8)+((8 + 1) × 1) = 129). The initial weights are randomly generated between −0.5 and +0.5. The ANN model weights are transformed between −4.48 and 4.39, after 8000 iterations, as shown in Fig. 3(a). We developed a standalone user interface design for analyzing the relationship between input

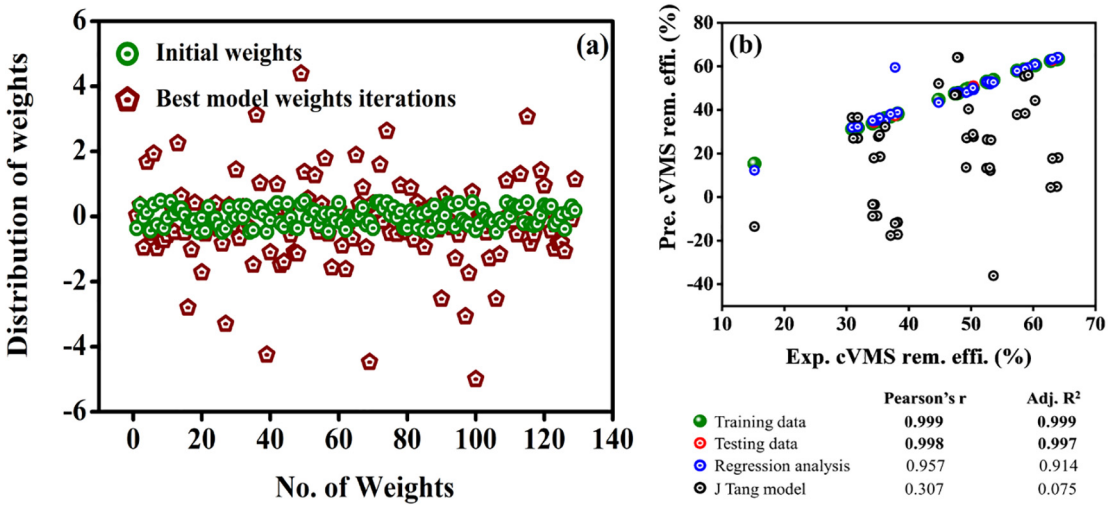

Fig. 3. (a) Distribution of initial and best model weights of the cVMSs removal efficiency. (b) Validation of the ANN model: training, testing datasets, regression analysis, and J Tang model quadratic equation with experimental cVMSs removal efficiency.

variables and cVMSs removal efficiency by using this architecture and final weights.

3.2. ANN model performance

After developing the model, the model performance was studied with correlation coefficients such as Pearson's r and Adj. R^2 values between experimental and predicted cVMSs removal efficiency of trained and tested datasets. Comparing the ANN model predicted cVMSs removal efficiency with experimental and previously published J Tang model (Tang et al., 2020) of the same data is shown in Fig. 3(b). The quadratic equation suggested by J Tang et al for calculating the cVMSs removal efficiency of wastewater given as

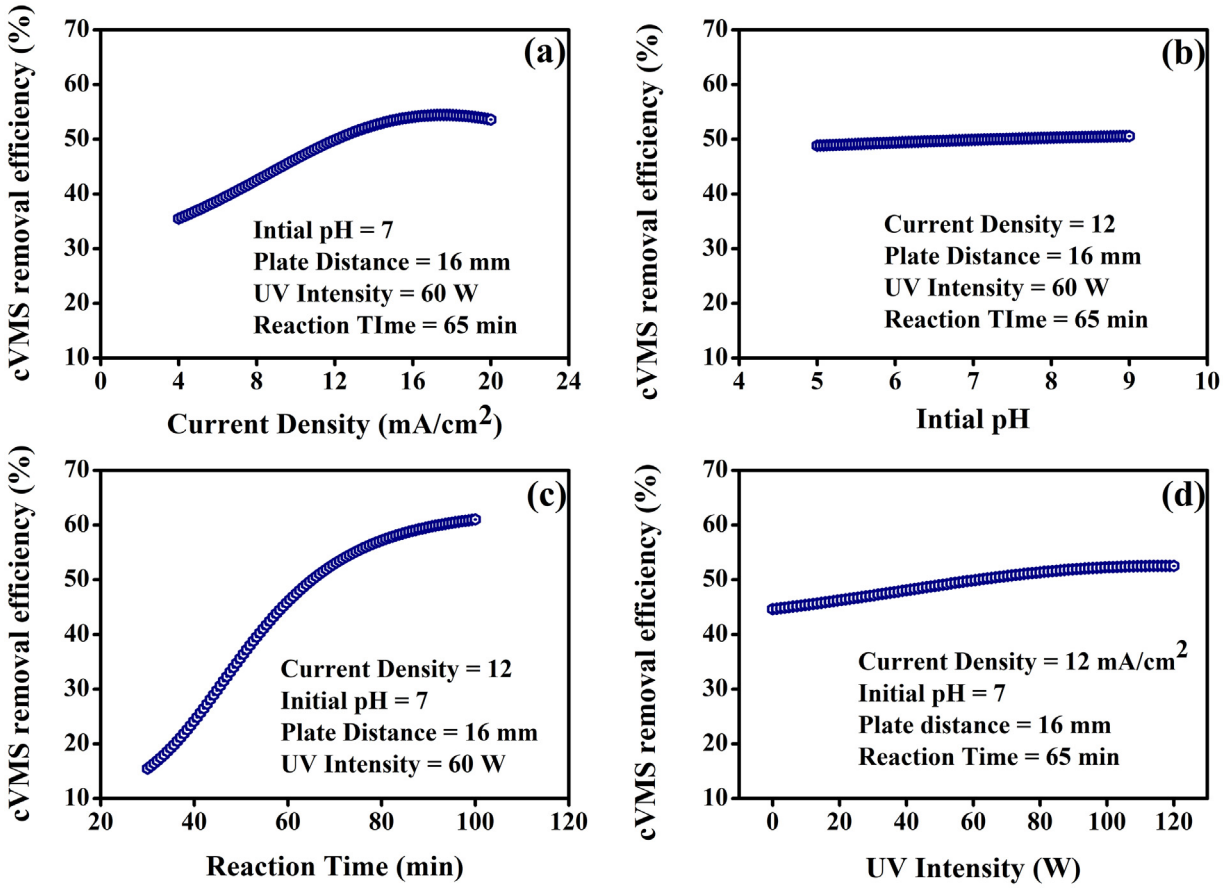

Fig. 4. ANN model predicted cVMSs removal efficiency as a function of (a) current density, (b) initial pH, (c) reaction time, and (d) UV intensity.

$$R_{cVMSs}\ (\%) = -63.45 + 0.688X_1 + 4.714X_2 + 0.7767X_3 + 0.087X_4 + 1.589X_5 + 0.0586X_1X_2 + 0.0086X_1X_3 - 0.0063X_1X_4 + 0.036X_1X_5 + 0.0056X_2X_3 - 0.0022X_2X_4 - 0.0025X_2X_5 - 0.0063X_3X_4 + 0.0016X_3X_5 + 0.0014X_4X_5 - 0.104X_1^2 - 0.362X_2^2 - 0.029X_3^2 - 0.0058X_4^2 - 0.011X_5^2$$

X1, X2, X3, X4, and X5 represent the current density, initial pH, plate distance, UV intensity, and reaction time.

Pearson's r, and Adj. R^2 values for testing, training, and J Tang quadratic equation of the same data were represented in Fig. 3 (b). The ANN model outperformed compared to other models in estimating the cVMSs removal efficiency with higher values of Pearson's r (0.999) and Adj. R^2 (0.997). From these results, we can conclude that the accurate prediction of cVMSs removal efficiency using ANN will help map the relationship between process parameters and removal efficiency.

4. Influence of process parameters on cVMSs removal efficiency (%)

4.1. Two-dimensional (2D) line plots

The effect of the process variables on cVMSs removal efficiency with keeping other variables at a constant value and the interactions between the parameters were revealed using the two-dimensional (2D) single variable plots as shown in Fig. 4. Fig. 4(a) shows the cVMSs removal efficiency was increased with increasing the current density up to 16 mA/cm^{2,} and further, the change is insignificant. This is due to the increase in hydroxyl radicals (·OH) results in the generation of holes due to the transfer of photo-generated carriers. However, the high current density leads to an improved voltage and the redistribution between the Helms's and space electric charge layers; thus, the cVMSs removal efficiency was decreased, and the predictions were in agreement with earlier reports (İrdemez et al., 2006; Sadeghi et al., 2014).

The pH of the solution was varied from 5 to 9 to study the effect of pH variation on the cVMSs removal efficiency. As shown in Fig. 4 (b), the removal efficiency of cVMSs marginal increase with pH was due to the formation of polymeric species and precipitation of Zn $((OH)_3$. (Chen et al., 2013; Wang et al., 2014). Fig. 4(c) shows that with the increase of reaction time from 30 to 100 min, the cVMSs removal efficiency was drastically increased. As reported in (Awual, 2019; Whelan, 2013), upon a long time, exposure of ZnO catalyst to UV light may generate more ·OH for oxidation due to overvoltage, which tends to increase the cVMSs removal efficiency. Fig. 4(d) shows that when the UV intensity varied from 0 to 90 W, the cVMSs removal efficiency was gradually increased. Due to the intense UV light, the photodegradation capability of ZnO was

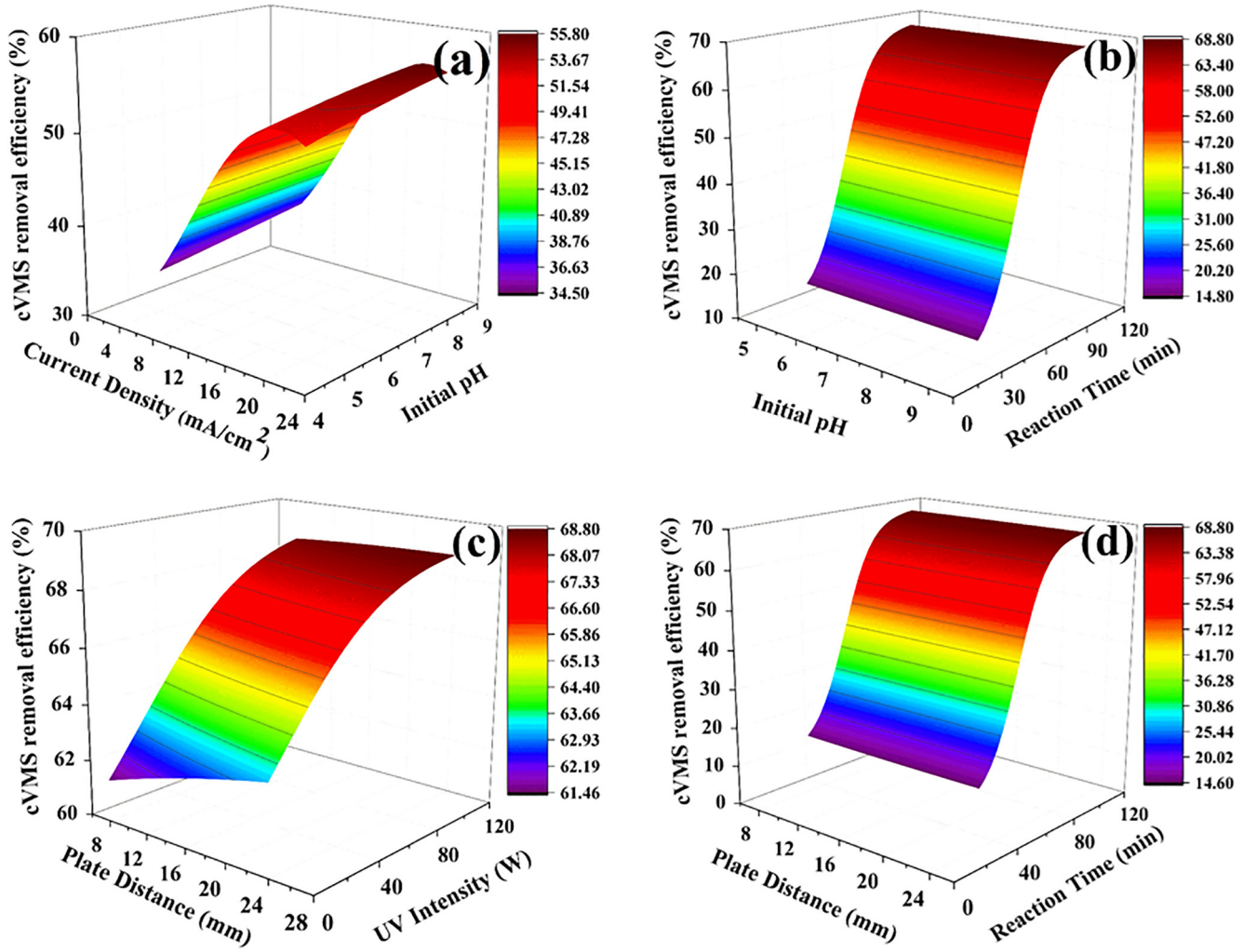

Fig. 5. Predicted cVMSs removal efficiency (a) current density & initial pH, (b) initial pH & reaction time, (c) plate distance & UV intensity, and (d) plate distance & reaction time.

increased. Furthermore, ZnO can absorb more photons and cause the formation of negative active electrons. Meanwhile, catalytic centers and holes were created in the valence bond to promote the catalytic oxidation reaction (Farnane et al., 2017; Lindenauer and Darby, 1994; Shirazian et al., 2017). The improved catalytic oxidation reaction can increase cVMSs removal efficiency.

4.2. Three-dimensional (3D) surface plots

The effect and relationship between the process parameters and cVMSs removal efficiency were showed by using 3D-plots, as depicted in Fig. 5. In each 3D-plot, two parameters were changed while the other three process variables were kept at constant values. Fig. 5(a) shows that the current density and initial pH was adjusted with the constant values of UV intensity(60 W), plate distance(24 mm), and reaction time(65 min). The cVMSs removal efficiency increases current density up to 16 mA/cm^2 due to the high generation of ·OH, in holes. After 16 mA/cm^2, the cVMSs removal efficiency was decreased due to the high current density, leading to high voltage. The decreased cVMSs removal efficiency is due to the redistribution of space between the Helms layer and the electric charge layer. While the initial pH increased, the cVMSs removal also increased as the Zn anode was precipitated. Zn $(OH)_3$ can lead to oxidation (Chen et al., 2013). Fig. 5(b) illustrates the combined effect of initial pH and reaction time on cVMSs removal efficiency with the constant values of current density (20 mA/cm^2), plate distance (24 mm), and UV intensity (60 W). With the increase of reaction time, the cVMSs removal efficiency was increased drastically due to ZnO's exposure over a relatively long time.

Fig. 5(c and d) illustrates the combined effect of plate distance, reaction time (at constant values of current density (20 mA/cm^2), initial pH (9), and UV intensity (120 W)), and UV intensity (at constant values of current density (20 mA/cm^2), initial pH (9), and reaction time (100 mins)) effect on cVMSs removal efficiency. At minimum plate distance, the cVMSs removal efficiency was minimum. The maximum efficiency was observed at the larger plate distance and the higher UV intensity, as shown in Fig. 5 (c). If the plate distance is too small, it can cause a short circuit; we need to choose the optimal plate distance for increasing cVMSs removal efficiency (Chen et al., 2013; Hashim et al., 2020). High UV intensity can increase the formation of active electrons and the absorption capability of more photons. The increased active electron can lead to an increase in cVMSs removal efficiency. Similarly, the plate distance and reaction time combined can increase cVMSs removal efficiency more ·OH for oxidation, as shown in Fig. 5(d). Based on the obtained ANN model results, the suggested optimal parameters for the higher cVMSs efficiency (~68%) are 100 min reaction time, 17.68 mm plate distance, and 8.01 initial pH, 15.12 mA/cm^2 current density, and 120 W UV intensity.

4.3. Index of relative importance (I_{RI})

We employed the I_{RI} method to identify the qualitative influence of process parameters on the removal efficiency of cVMSs. The magnitude and nature of I_{RI} show the impact of the input parameters on the cVMSs removal efficiency. The I_{RI} calculations and explanations were reported in our previous work (Sadan et al., 2016). Fig. 6 shows the I_{RI} for cVMSs removal efficiency of 15.2 and 63.8%. Fig. 6(a) shows the lower values of current density and reaction time, which resulted in lower cVMSs removal efficiency. These two parameters are important input parameters for increasing the removal efficiency. The low current density and low reaction time can decrease the ·OH, generation for oxidation so that it can reduce the removal efficiency (Whelan, 2013). Fig. 6(b) shows the high cVMSs removal efficiency at current density, initial pH, and plate distance, and there were higher values for all the input variables (i.e., 15.4 mA/cm^2, 7.8, 12.6 mm, 80 W, and 80 min) and the corresponding removal efficiency was 63.5%. Due to the higher process variables, it could be attributed that there was an exposure of ZnO to high UV intensity and current density over a long reaction time, which can increase the ·OH for oxidation. From this I_{RI}, we can compare the effect of process variables on cVMSs removal efficiency following the order: Plate distance < initial pH < UV intensity < current density < reaction time.

4.4. Virtual cVMSs removal efficiency with mean values of experimental parameters

The predicted cVMSs removal efficiency for mean values of the experimental data was 15.16%. Table 2 shows the quantitative estimation of cVMSs removal efficiency by the virtual addition of input variables. To achieve experimental conditions of sample 25 (see Table S1), we changed the variables step by step and calculated the cVMSs removal efficiency quantitatively.

The current density was changed from 12 to 15.4 mA/cm^2 by keeping other variables constant at mean values, and the predicted cVMSs removal efficiency is 14.25%. The cVMSs removal efficiency was decreased due to the less reaction time (İrdemez et al., 2006). Next, we increased the initial pH from 7 to 7.8, and the predicted cVMSs removal efficiency was 14.65. The slight increase in efficiency is due to the increasing current density and initial pH. The increase in initial pH can lead to all the ·OH for oxidation (Chen et al., 2013). Later, we changed the plate distance from 16 to

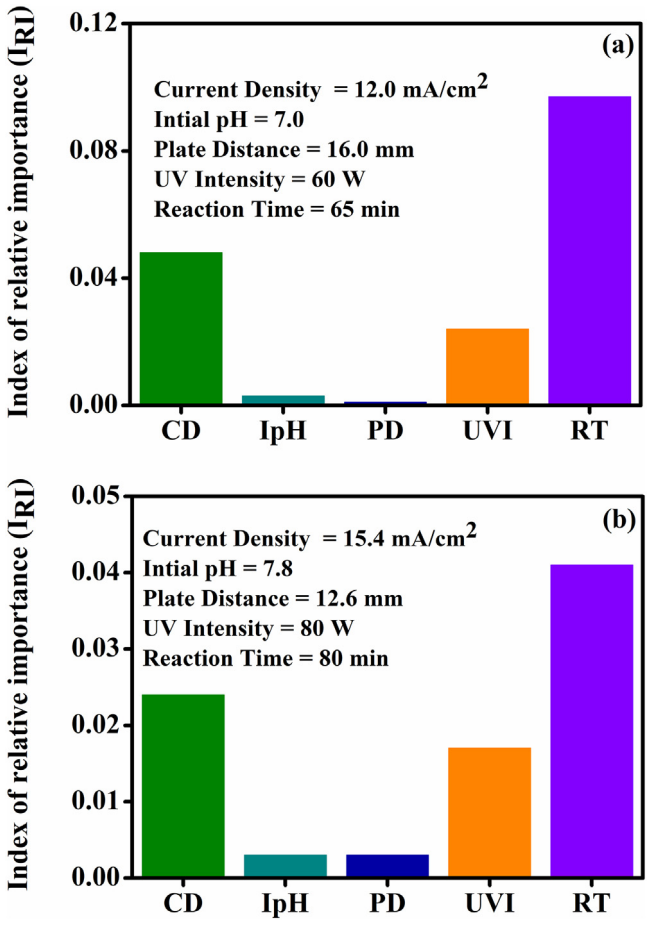

Fig. 6. The index of relative importance (I_{RI}) of process variables on cVMSs removal efficiency (%) (a) 15.2% and (b) 63.5%.

Table 2
cVMSs removal efficiency was calculated virtual system quantitatively.

Current density (mA/cm^2)	Initial pH	Plate Distance (mm)	UV Intensity (W)	Reaction Time (min)	cVMSs removal efficiency	Change in cVMSs removal efficiency
12	7	16	60	30	15.16	–
15.4	7	16	60	30	14.25	−0.91
15.4	7.8	16	60	30	14.65	0.4
15.4	7.8	19.4	60	30	14.60	−0.05
15.4	7.8	19.4	85	30	14.82	0.22
15.4	7.8	19.4	85	80	**63.43**	48.61

The experimental value of cVMSs removal efficiency for these conditions: **64.14**.

19.4 mm, and the predicted cVMSs removal efficiency was 14.60. Again, we modified the UV intensity 60 to 85 W and the prediction was 14.82. Finally, when we increased the reaction time from 30 to 80 min resulted in significant increase in removal efficiency to 63.55% where as the experimental removal efficiency for these conditions was 64.14.

5. Conclusion

In this work, we used the ANN method to model the relationship between cVMSs removal efficiency and its photo-electrocatalysis parameters (current density, initial pH, plate distance, UV intensity, and reaction time). The ANN model can predict the cVMSs removal efficiency for an unlimited new combination of process variables with good accuracy. The predicted train and test datasets adj. R^2 value for cVMSs removal is 0.997, and 0.999, respectively. The developed model successfully predicted the effect of single and two variables on cVMSs removal efficiency. We estimated the effect of each input variable on cVMSs removal efficiency quantitatively.

Declaration of Competing Interest

The authors declare that they have no known competing financial interests or personal relationships that could have appeared to influence the work reported in this paper.

Acknowledgment

N. S. Reddy acknowledges YSJ and MGR for the Inspiration. All the authors extend their appreciation to the Research Support Project (number RSP-2020/218), King Saud University, Riyadh, Saudi Arabia.

Appendix A. Supplementary data

Supplementary data to this article can be found online at https://doi.org/10.1016/j.jksus.2020.101339.

References

Alsamhary, K.I., 2020. Effects of salinity and wastewater on the growth of Synechococcus elongatus (strain PCC 7942) and some of its cellular components. J. King Saud Univ. – Sci. 32, 3293–3300.
Awual, M.R., 2019. An efficient composite material for selective lead(II) monitoring and removal from wastewater. J. Environ. Chem. Eng. 7, 103087.
Bletsou, A.A., Asimakopoulos, A.G., Stasinakis, A.S., Thomaidis, N.S., Kannan, K., 2013. Mass loading and fate of linear and cyclic siloxanes in a wastewater treatment plant in Greece. Environ. Sci. Technol. 47, 1824–1832.
Bramer, M., 2020. An introduction to neural networks. In: Principles of Data Mining. Springer, pp. 427–466.
Chen, X., Lin, H., Ren, H.Y., Xing, J.L., 2013. Experimental study on wastewater treatment containing copper with electrodeposition method. Adv. Mater. Res. Trans. Tech. Publ., 1670–1673
Di, Z., Chang, M., Guo, P., Li, Y., Chang, Y., 2019. Using Real-Time Data and Unsupervised Machine Learning Techniques to Study Large-Scale Spatio-Temporal Characteristics of Wastewater Discharges and their Influence on Surface Water Quality in the Yangtze River Basin. Water 11, 1268.
Durán, I.R., Profili, J., Stafford, L., Laroche, G., 2020. Unveiling the origin of the anti-fogging performance of plasma-coated glass: Role of the structure and the chemistry of siloxane precursors. Prog. Org. Coat. 141, 105401.
Farnane, M., Tounsadi, H., Elmoubarki, R., Mahjoubi, F., Elhalil, A., Saqrane, S., Abdennouri, M., Qourzal, S., Barka, N., 2017. Alkaline treated carob shells as sustainable biosorbent for clean recovery of heavy metals: Kinetics, equilibrium, ions interference and process optimisation. Ecol. Eng. 101, 9–20.
Gadekar, M.R., Ahammed, M.M., 2019. Modelling dye removal by adsorption onto water treatment residuals using combined response surface methodology-artificial neural network approach. J. Environ. Manage. 231, 241–248.
Guo, J., Zhou, Y., Zhang, B., Zhang, J., 2019. Distribution and evaluation of the fate of cyclic volatile methyl siloxanes in the largest lake of southwest China. Sci. Total Environ. 657, 87–95.
Hashim, K.S., Kot, P., Zubaidi, S.L., Alwash, R., Al Khaddar, R., Shaw, A., Al-Jumeily, D., Aljefery, M.H., 2020. Energy efficient electrocoagulation using baffle-plates electrodes for efficient Escherichia coli removal from wastewater. J. Water Process Eng. 33, 101079.
Hernández-del-Olmo, F., Gaudioso, E., Duro, N., Dormido, R., 2019. Machine Learning Weather Soft-Sensor for Advanced Control of Wastewater Treatment Plants. Sensors 19, 3139.
Hori, H., Kakizawa, T., Kuriyama, N., Kabuki, A., Otsuki, M., Horii, Y., 2019. Decomposition of environmentally persistent cyclic methylsiloxanes in subcritical water. Sustainable Chem. Pharm. 13, 100160.
İrdemez, Ş., Demircioğlu, N., Yıldız, Y.Ş., Bingül, Z., 2006. The effects of current density and phosphate concentration on phosphate removal from wastewater by electrocoagulation using aluminum and iron plate electrodes. Sep. Purif. Technol. 52, 218–223.
LeCun, Y., Bengio, Y., Hinton, G., 2015. Deep learning. Nature 521, 436–444.
Li, C.-L., Narayana, P., Reddy, N., Choi, S.-W., Yeom, J.-T., Hong, J.-K., Park, C.H., 2019. Modeling hot deformation behavior of low-cost Ti-2Al-9.2 Mo-2Fe beta titanium alloy using a deep neural network. J. Mater. Sci. Technol. 35, 907–916.
Lindenauer, K.G., Darby, J.L., 1994. Ultraviolet disinfection of wastewater: effect of dose on subsequent photoreactivation. Water Res. 28, 805–817.
Lippmann, R., 1987. An introduction to computing with neural nets. IEEE ASSP Mag. 4, 4–22.
Maurya, A., Narayana, P., Bhavani, A.G., Jae-Keun, H., Yeom, J.-T., Reddy, N., 2020. Modeling the relationship between electrospinning process parameters and ferrofluid/polyvinyl alcohol magnetic nanofiber diameter by artificial neural networks. J. Electrostat. 104, 103425.
Newhart, K.B., Marks, C.A., Rauch-Williams, T., Cath, T.Y., Hering, A.S., 2020. Hybrid statistical-machine learning ammonia forecasting in continuous activated sludge treatment for improved process control. J. Water Process Eng. 37, 101389.
Reddy, B.R.S., Premasudha, M., Panigrahi, B.B., Cho, K.-K., Reddy, N.G.S., 2020. Modeling constituent–property relationship of polyvinylchloride composites by neural networks. Polym. Compos. 41, 3208–3217.
Reddy, N., Krishnaiah, J., Young, H.B., Lee, J.S., 2015. Design of medium carbon steels by computational intelligence techniques. Comput. Mater. Sci. 101, 120–126.
Sadan, M.K., Ahn, H.-J., Chauhan, G., Reddy, N., 2016. Quantitative estimation of poly (methyl methacrylate) nano-fiber membrane diameter by artificial neural networks. Eur. Polym. J. 74, 91–100.
Sadeghi, S., Alavi Moghaddam, M.R., Arami, M., 2014. Improvement of electrocoagulation process on hexavalent chromium removal with the use of polyaluminum chloride as coagulant. Desalin. Water Treat. 52, 4818–4829.
Shirazian, S., Kuhs, M., Darwish, S., Croker, D., Walker, G.M., 2017. Artificial neural network modelling of continuous wet granulation using a twin-screw extruder. Int. J. Pharm. 521, 102–109.
Shukla, P., Sun, H., Wang, S., Ang, H.M., Tadé, M.O., 2011. Co-SBA-15 for heterogeneous oxidation of phenol with sulfate radical for wastewater treatment. Catal. Today 175, 380–385.
Tang, J., Zhang, C., Wang, L., Hu, Y., Su, P., Wang, W., He, X., 2020. Photo-electrocatalytic degradation of cyclic volatile methyl siloxane by ZnO-coated aluminum anode: Optimal parameters, kinetics, and reaction pathways. Sci. Total Environ. 733, 139246.
Wang, J., Zhang, W., Xu, J., Li, Y., Xu, X., 2014. Octamethylcyclotetrasiloxane removal using an isolated bacterial strain in the biotrickling filter. Biochem. Eng. J. 91, 46–52.
Whelan, M., 2013. Evaluating the fate and behaviour of cyclic volatile methyl siloxanes in two contrasting North American lakes using a multi-media model. Chemosphere 91, 1566–1576.